JOURNAL OF PETROLOGY | VOLUME 44 | NUMBER 9 | PAGES 1561–1578 | 2003 | Doi: 10.1093/Petrology/egg049

The Petrology and Geochemistry of High-Magnesium Andesites at the Western Tip of the Setouchi Volcanic Belt, SW Japan

Y. TATSUMI[1]*, H. SHUKUNO[1], K. SATO[1], T. SHIBATA[1,2] AND M. YOSHIKAWA[1,2]

[1]INSTITUTE FOR FRONTIER RESEARCH ON EARTH EVOLUTION (IFREE), JAPAN MARINE SCIENCE AND TECHNOLOGY CENTER (JAMSTEC), YOKOSUKA 237-0061, JAPAN

[2]INSTITUTE FOR GEOTHERMAL SCIENCES, KYOTO UNIVERSITY, BEPPU 874-0907, JAPAN

RECEIVED MAY 31, 2003; ACCEPTED MARCH 11, 2003

K–Ar ages, and petrographical and geochemical characteristics of high-magnesium andesites and plagioclase-phyric andesites from the NE Kyushu region, Japan, are presented. K–Ar ages range from 10·7 ± 0·3 to 14·4 ± 0·4 Ma, overlapping those reported for lavas of the Setouchi Volcanic Belt in other regions (11–16 Ma). This, together with major and incompatible trace element, and Sr–Nd–Pb isotopic characteristics, confirms that the Setouchi Volcanic Belt, which is characterized by the occurrence of high-magnesium andesites, extends for ~600 km along the SW Japan arc. Thus, it may be suggested that the unusual tectonic setting required for high-magnesium andesite magma generation was attained only for this limited region, possibly in association with subduction of the young, hence hot, lithosphere of the Shikoku Basin. Two types of high-magnesium andesite, possessing identical bulk-rock compositions, are recognized: one contains olivine phenocrysts with chromian spinel inclusions showing compositional characteristics consistent with their crystallization as liquidus phases, whereas the other contains Ni- and Fe-rich olivine and Fe^{3+}-rich spinel. One of the possible causes for such unusual mineral compositions could be effective elemental diffusion within and through olivine crystals associated with a long residence time in a crustal magma chamber and the slow rate of cooling of the host magma. The compositions of liquidus chromite and olivine, as well as whole-rock major element compositions, suggest that the NE Kyushu high-magnesium andesite magmas were produced by higher degrees of partial melting than those in other regions of the Setouchi Volcanic Belt.

KEY WORDS: *Setouchi Volcanic Belt; NE Kyushu; high-Mg andesites*

INTRODUCTION

High-magnesium andesites (HMAs), with high MgO contents and/or high Mg/Fe ratios, are volumetrically rare in the modern Earth. They are, however, important rock types, as the production of HMAs in the Earth's early history could have contributed greatly to continental crust formation (Kelemen, 1995). The reasons for believing so are twofold. First, the bulk continental crust has an andesitic composition (Christensen & Mooney, 1995; Rudnick & Fountain, 1995; Taylor & McLennan, 1995). Second, HMAs, which form a recognizable part of the continental crust as monzodioritic and trachyandesitic rocks in Archaean cratons, may differentiate to produce more evolved andesites with compositions broadly identical to the continental crust (Shirey & Hanson, 1984; Stern *et al.*, 1989; Stern & Hanson, 1991).

Solely on the basis of its major element composition, an HMA magma could be produced from a parental basalt magma through an assimilation–fractional crystallization process within the crust. However, the petrographical, trace element, and isotopic characteristics of HMAs and associated basalts do not support such a process (e.g. Tatsumi & Ishizaka, 1982; Suzuki

*Corresponding author. Telephone: 81-468-67-9760. Fax: 81-467-67-9625. E-mail: tatsumi@jamstec.go.jp

& Tatsumi, 2003). The characteristic high Mg/Fe ratios in HMAs, on the other hand, provide evidence for their equilibration with upper-mantle peridotites (Sato, 1977; Kuroda *et al*., 1978; Jenner, 1981; Crawford *et al*., 1989). Experimental work has demonstrated that partial melting of peridotites in the upper mantle can yield high-SiO_2 and high-Mg melts under hydrous conditions (Kushiro, 1969; Tatsumi, 1981, 1982; Hirose, 1997). Such experimental results led Crawford *et al*. (1989) and Tatsumi & Maruyama (1989) to the conclusion that hydrous melting of upper-mantle peridotites, triggered by direct addition of slab-derived aqueous fluids, is a likely mechanism of HMA magma production in subduction zones. On the other hand, a mechanism including the reaction between hydrous silicic partial melts, derived from the subducting oceanic crust and/or sediments, and overlying mantle wedge peridotites has recently attracted attention (Kay, 1978; Pearce *et al*., 1992; Yogodzinski *et al*., 1994; Kelemen, 1995; Shimoda *et al*., 1998; Tatsumi, 2001).

In most arc–trench systems on the modern Earth, however, basalt not HMA magmas are generated in the mantle wedge as a consequence of plate subduction (e.g. Tatsumi & Eggins, 1995). It is thus intuitively expected that some unusual tectonic conditions must exist for the production of HMA magmas. Knowledge of the tectonic setting of a volcanic belt in which HMA magmatism has occurred is, therefore, essential to improve our understanding of the origin of HMAs and, additionally, that of the continental crust. It may be also interesting to examine the limits of such unusual volcanism, to reconstruct the original tectonic setting. This paper presents K–Ar ages, petrographical and geochemical characteristics of volcanic rocks, including HMAs, from the NE part of Kyushu, SW Japan; these data provide evidence for the extension of the Setouchi Volcanic Belt, which is characterized by the occurrence of HMAs, to this region.

GEOLOGICAL SETTING AND SAMPLES

The Setouchi Volcanic Belt (SVB) is located in the present forearc region of the SW Japan arc, ~80 km south of the Quaternary volcanic front. It extends possibly for 600 km with five major volcanic regions (Fig. 1): Shitara, Osaka, NE and NW Shikoku and NE Kyushu towards the west. Formation of the SVB parallel to the arc–trench system may indicate the involvement of the subducting lithosphere of the Shikoku Basin in producing the SVB magmas. New K–Ar age data for the SVB lavas (Tatsumi *et al*., 2001) have confirmed an earlier suggestion (Tatsumi, 1983)

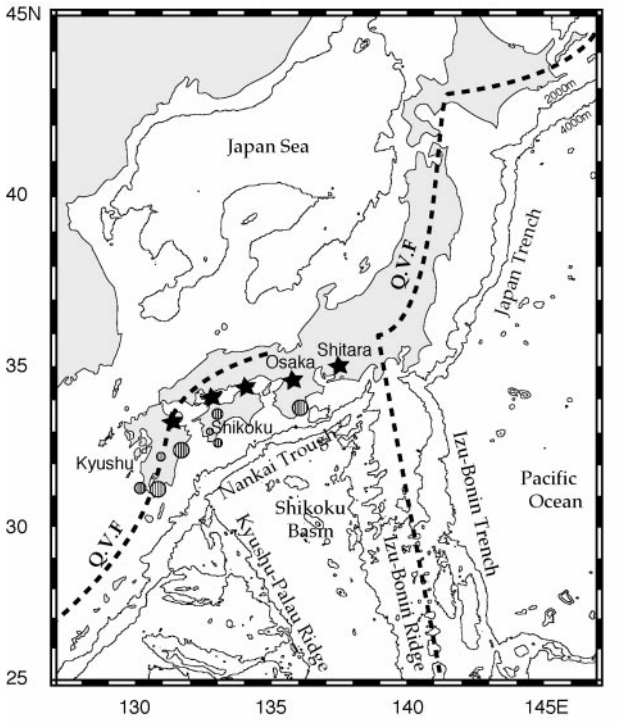

Fig. 1. Location of the Setouchi Volcanic Belt (stars) in the present forearc of the SW Japan arc, i.e. at the trench side of the Quaternary volcanic front (Q.V.F.). Bathymetric contours are given in 2000 m intervals. Felsic volcano-plutonic complexes, which formed synchronously with the Setouchi Volcanic Belt, occur in the near-trench region of the SW Japan arc (hatched).

that Setouchi magmatism took place within a short period from 11 to 16 Ma. This is largely synchronous with the timing of a 40–50° clockwise rotation of the arc sliver of SW Japan or the major phase of rifting of the Japan Sea back-arc basin at 14–16 Ma (Otofuji *et al*., 1991). It has been suggested that southward drift of the SW Japan arc, caused by the clockwise rotation of the arc sliver, resulted in the subduction of the very young (~15 Ma; Okino *et al*., 1994; Tamaki *et al*., 1999) oceanic crust of the Shikoku Basin beneath the arc lithosphere (Tatsumi & Maruyama, 1989).

Felsic volcanic–plutonic complexes occur in the near-trench region (Outer Zone) of the SW Japan arc (Fig. 1); these intruded into an accretionary prism built in the Cretaceous to Miocene period. K–Ar ages of these complexes concentrate in the range 12–15 Ma (Shibata, 1978; Sumii, 2000), synchronous with the SVB magmatism. Shinjoe (1997) proposed that such near-trench magmatism was caused by melting of sediments in the accretionary prism under unusually high-temperature conditions.

The NE Kyushu region has been proposed as the western edge of the SVB because of the occurrence of Miocene volcanic rocks with macroscopic features

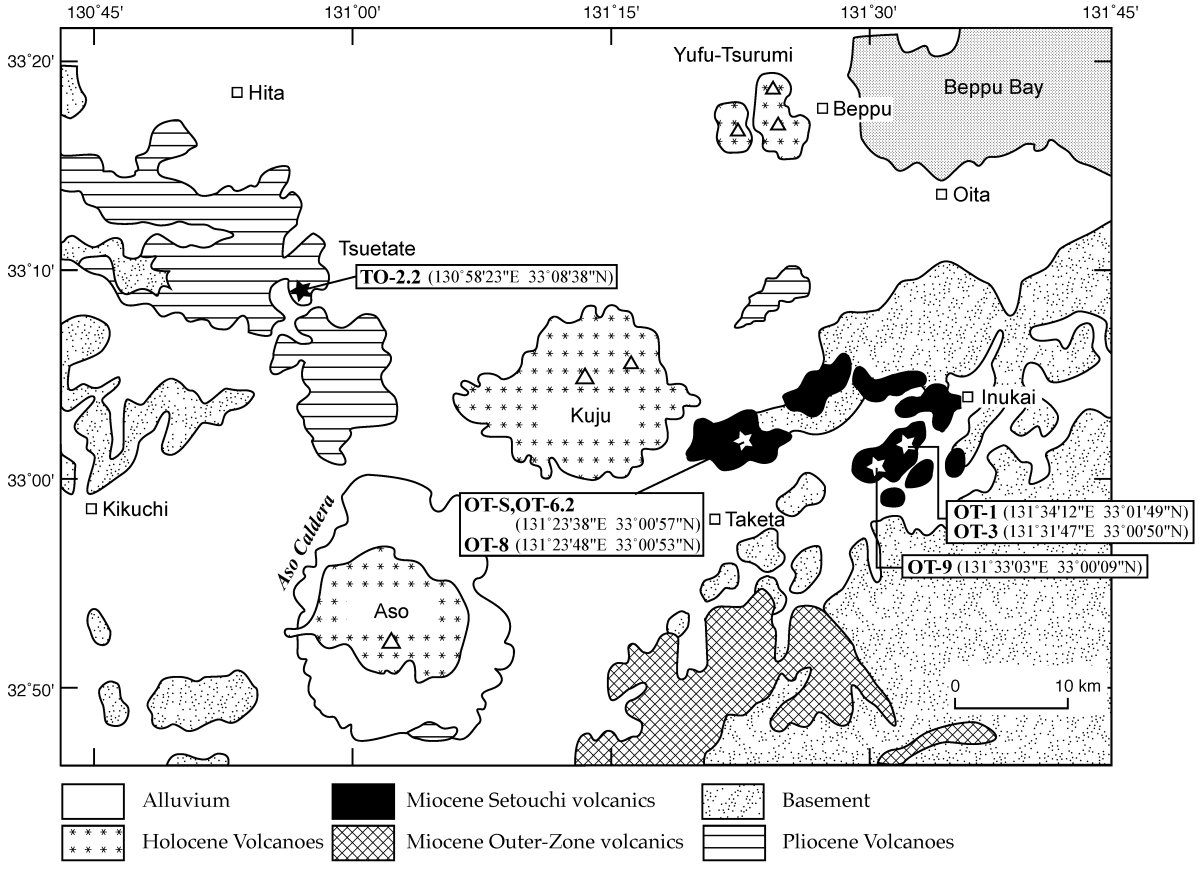

Fig. 2. Distribution of Cenozoic volcanic rocks in the NE Kyushu region (after Kamata, 1985). Sampling localities (stars) and their longitudes and latitudes are also shown. Five samples were collected from Miocene lavas and a dyke, and one sample (TO-2.2) from Pliocene volcanics.

similar to those of the central regions of the SVB, such as aphyric glassy andesites termed sanukitoids (Tatsumi, 1983). This is supported by available K–Ar age data for these volcanic rocks, ranging from 10 to 14 Ma (Shibata & Ono, 1974; Tatsumi *et al.*, 1980; Shiraki *et al.*, 1995). Miocene volcanic rocks from NE Kyushu (Fig. 2), referred to as the Ohno volcanic rocks (Ono, 1963), are composed mainly of andesitic lava flows, rhyolitic welded tuffs, pyroclastic flows and tuffs. They cover the basement rocks, including Jurassic metamorphic rocks, and are unconformably overlain by nonmarine, Plio-Pleistocene deposits, the Sekinan Group.

To re-examine the age of the magmatism and to compare the petrographical and geochemical signatures of NE Kyushu rocks with those of SVB lavas in other regions, four glassy andesite samples (OT-1, -3, -8, and -9) were collected from the Daisango-Yama lava flow (Fig. 2). Ono (1963) reported the presence of a dyke of 10 m width intruding rhyolitic welded tuffs with a strike of N60°W and a dip of 70°NE. Two samples, OT-6.2 and OT-S, were collected from the central part of this dyke and from a fallen block near the dyke, respectively (Fig. 2). To reveal the distinctive geochemical characteristics of the SVB volcanics in this region, a mafic andesite (TO-2.2) was also collected from the Plio-Pleistocene Maji andesite lava flow (Kamata, 1985), which is located ~30 km west of the Ohno volcanic rocks (Fig. 2).

EXPERIMENTAL METHODS

The rock samples for K–Ar dating were crushed and sieved into a 60–80 mesh size fraction. Phenocryst minerals were removed by hand-picking. A groundmass fraction was used for argon analysis. A portion of this fraction was ground in an agate mortar for potassium analysis. Analyses of potassium and argon, and calculations of ages and errors were carried out following the methods described by Nagao *et al.* (1984) and Matsumoto (1989). Potassium was analysed by flame emission photometry using a lithium internal

standard and peak integration method. The analytical error is within 2% at the 1σ confidence level. Argon was analysed by mass spectrometry using a 15 cm radius sector type instrument with a single-collector system, using an isotope dilution method and a ^{38}Ar spike (Saito, 1989; Takaoka, 1989). Multiple runs of a standard sample (HD-B1 biotite, 25 Ma) indicate that the error in the argon analysis is ~1% at the 1σ confidence level. The decay constants for ^{40}K to ^{40}Ar and ^{40}Ca, and ^{40}K content of potassium used in the age calculations are from Steiger & Jager (1977) and are $0{\cdot}581 \times 10^{-10}$/year, $4{\cdot}962 \times 10^{-10}$/year and $1{\cdot}167 \times 10^{-4}$, respectively.

Major and trace element (Rb to Ni in Table 1) compositions were measured by X-ray fluorescence (XRF) spectrometry using RIGAKU® Simaltics 3550 and Rix 3000 systems, on fused glass beads and pressed powder pellets, respectively. Detailed analytical procedures have been described by Goto & Tatsumi (1994, 1996). Concentrations of rare earth elements, Co, Cr, and Sc were determined by instrumental neutron activation analysis following the procedures described by Masuda *et al.* (1974).

Rock samples for Sr–Nd–Pb isotope analysis were crushed to coarse chips (<0·5 cm^3) and fresh pieces were hand-picked. To avoid surface contamination the rock chips were then leached with 0·5 M HCl at room temperature for 1 h. The chips were ground to less than 200 mesh size using a vibration mill made of alumina ceramic. The analytical procedure for chemical separation and mass spectrometry for Sr, Nd and Pb isotope determinations has been outlined by Yoshikawa *et al.* (2001) and Shibata *et al.* (in prep.). Total procedural blanks for Sr, Nd and Pb were <100 pg, <10 pg and <2 pg, respectively. Mass spectrometry was performed on a Thermo-Finnigan® MAT261 system equipped with nine Faraday cups, using a static multi-collection mode. Normalizing factors to correct for isotopic fractionation in Sr, Nd and Pb isotope analyses are $^{86}Sr/^{88}Sr = 0{\cdot}1194$, $^{146}Nd/^{144}Nd = 0{\cdot}7219$, and 0·116% per atomic mass unit, respectively. Measured isotopic ratios for standard materials were $^{87}Sr/^{86}Sr = 0{\cdot}710279 \pm 28$ (2σ) for NBS987 ($n = 5$); $^{143}Nd/^{144}Nd = 0{\cdot}511851 \pm 13$ for La Jolla ($n = 9$); and $^{206}Pb/^{204}Pb = 16{\cdot}938 \pm 0{\cdot}003$, $^{207}Pb/^{204}Pb = 15{\cdot}494 \pm 0{\cdot}004$, and $^{208}Pb/^{204}Pb = 37{\cdot}708 \pm 0{\cdot}011$ for NBS981 ($n = 8$).

Mineral compositions were determined by electron-probe micro-analysis using JEOL® JXA-8800 and -8900 systems. The excitation potential, specimen current, and analytical time were: 20 kV, 25 nA, and 20 s (100 s for Mn, Ca, and Ni) for olivine; 15 kV, 12 nA, and 20 s for spinel; and 15 kV, 15 nA, and 20 s for pyroxene and plagioclase. ZAF correction procedures were employed.

RESULTS

Major and trace element, Sr–Nd–Pb isotopic, and modal compositions of the andesite samples, and the results of K–Ar dating are listed in Table 1, together with compositions of representative HMAs and basalt in the SVB. Representative mineral compositions are given in Tables 2–6.

K–Ar ages

There is microscopic evidence for minor alteration in all of the studied samples. Olivine phenocrysts in both OT-6.2 and OT-S are partly (~30%) replaced by serpentine, chlorite, and unidentifiable clay minerals. Although OT-1 and OT-9 are relatively fresh, other samples contain clay minerals in the groundmass. Such alteration may cause significant contamination by atmospheric argon (>50%) in these samples (Table 1).

Tatsumi *et al.* (2001) reported a total of 50 K–Ar ages for lavas and dykes from the Osaka and NE Shikoku regions of the SVB. These data, together with other recent age determinations by Uto *et al.* (1996), Sumii (2000), Shinjoe & Sumii (2001), and Shimada *et al.* (2001), confirmed that Setouchi magmatism took place between 11 and 16 Ma. The new K–Ar age data obtained as part of this study are consistent with those for Setouchi volcanic rocks in other regions (Fig. 3), providing evidence for the extension of the SVB to the NE Kyushu region. The Plio-Pleistocene andesite gave a K–Ar age of $1{\cdot}88 \pm 0{\cdot}16$ Ma, confirming the eruption of this lava during the Quaternary.

Mineral and bulk-rock compositions

Two andesites (OT-S and OT-6.2) among seven analysed samples are characterized by the absence of plagioclase phenocrysts, which typify HMAs and associated near-aphyric andesites (sanukitoids) in the SVB. These rocks are also distinct in their high MgO contents compared with average orogenic andesite (Table 1). If we normalize the major element compositions to 100% on a volatile-free basis, then SiO_2 contents for those samples are ~54 wt %. Thus, these Mg-rich rocks can be classified as HMAs, although they should, in a strict sense, be termed basaltic andesites. Although the 100%-normalized major element compositions of such HMAs are similar, the constituent minerals show marked differences in composition. Olivine phenocrysts in HMA OT-S are more magnesian and characterized by a narrower compositional range than those in HMA OT-6.2, whereas the compositions of clinopyroxene phenocrysts are identical in both (Fig. 4a, b, d, and e). The NiO content at a given Mg/(Mg + Fe) of olivine phenocrysts in HMA

Table 1: Major and trace element, Sr–Nd–Pb isotopic, and modal compositions, and results of K–Ar dating

Sample:	OT-1	OT-3	OT-8	OT-9	OT6·2	OT-S	TO-2.2	SD-261[3]	TGI-5[3]	NBY-5[3]	SDSYB[3]
Rock type:	PA[1]	PA	PA	PA	HMA[2]	HMA	PA	cpx-HMA	opx-HMA	ol-rich HMA	basalt
wt %											
SiO_2	60·79	60·63	61·24	59·45	51·68	53·18	54·97	55·37	57·27	55·86	48·95
TiO_2	1·22	1·21	1·23	1·15	0·93	0·94	1·10	0·65	0·42	0·40	1·02
Al_2O_3	16·94	16·97	17·21	16·93	13·68	14·36	18·50	15·55	14·26	14·25	14·69
$Fe_2O_3^*$	5·99	5·80	5·76	6·57	8·36	9·70	8·53	6·92	6·19	6·86	10·21
MnO	0·12	0·10	0·10	0·11	0·13	0·15	0·15	0·17	0·12	0·12	0·17
MgO	1·44	1·49	1·46	2·32	10·19	8·64	3·15	6·89	9·45	10·95	11·79
CaO	5·76	5·74	5·76	6·20	7·52	7·84	8·23	7·04	6·31	7·11	8·75
Na_2O	3·05	3·02	3·12	2·97	2·41	2·17	3·25	2·84	2·57	2·32	2·57
K_2O	2·96	2·85	2·98	2·26	1·39	1·28	1·33	2·25	1·16	1·12	1·20
P_2O_5	0·26	0·26	0·26	0·22	0·19	0·19	0·27	0·17	0·1	0·11	0·27
Total	98·53	98·07	99·10	98·18	96·47	98·45	99·49	97·85	97·85	99·10	99·62
ppm											
Rb	98	99	100	80	46	66	30	114	45	48	33
Ba	479	462	467	348	297	359	373	195	336	378	219
Th	8·8	8·6	8·6	7·0	3·4	4·2	3·2	4·8	4·9	3·0	4·2
Nb	12	12	12	10	6	6	9	5	3	2	4
Pb	17	17	16	15	7	10	7	17	13	11	8
Sr	283	287	283	271	265	331	623	267	308	284	277
Zr	232	231	232	184	114	118	116	80	94	68	99
Y	23	23	23	20	14	37	26	15	11	11	18
Ni	9·3	9·2	9·1	6·6	208	234	0·9	148	179	254	207
La	25·3	27·7	25·6	21·4	14·1	15·8	20·9	9·17	12·2	9·49	10·9
Ce	52·1	56·2	57·2	50·0	33·7	59·4	54·6	21·6	22·5	18·2	21·1
Sm	5·00	6·00	5·47	4·79	3·51	3·62	4·58	2·48	2·37	2·04	3·80
Eu	—	1·68	1·42	1·26	0·98	1·03	1·73	0·85	0·69	0·62	1·23

Table 1: continued

Sample:	OT-1	OT-3	OT-8	OT-9	OT6·2	OT-S	TO-2.2	SD-261[3]	TGI-5[3]	NBY-5[3]	SDSYB[3]
Rock type:	PA[1]	PA	PA	PA	HMA[2]	HMA	PA	cpx-HMA	opx-HMA	ol-rich HMA	basalt
Tb	0·69	0·77	0·68	0·57	0·48	0·52	0·69	0·49	0·40	0·32	0·68
Yb	2·16	2·30	2·66	2·14	1·88	1·88	2·25	1·55	1·49	1·38	1·86
Lu	0·30	0·36	0·33	0·29	0·30	0·32	0·35	0·26	0·21	0·21	0·28
Co	18·6	17·7	17·9	17·6	43·5	43·6	22·7	31·7	34·5	41·1	51·1
Cr	29	27	26	30	595	576	14	342	534	535	541
Sc	15·8	17·2	16·8	21·4	25·8	26·4	23·4	22·1	22·8	27·4	30·3
$^{87}Sr/^{86}Sr$	0·706767 ± 04	0·706735 ± 03	0·706753 ± 03	0·706588 ± 04	0·705527 ± 03	0·705639 ± 10	0·704289 ± 04				
$(^{87}Sr/^{86}Sr)_i$[4]	0·70661	0·70656	0·70661	0·70644	0·705435	0·705555	0·704285	0·70490	0·70514	0·70537	0·70439
$^{143}Nd/^{144}Nd$	0·512413 ± 09	0·512418 ± 09	0·512411 ± 04	0·512413 ± 04	0·512510 ± 04	0·512506 ± 08	0·512648 ± 09	0·512700	0·512588	0·512533	0·512747
$^{206}Pb/^{204}Pb$	18·410 ± 05	18·375 ± 02	18·418 ± 05	18·359 ± 05	18·330 ± 04	18·333 ± 01	18·386 ± 02	18·369	18·450	18·425	18·314
$^{207}Pb/^{204}Pb$	15·609 ± 04	15·572 ± 01	15·620 ± 04	15·603 ± 04	15·557 ± 03	15·583 ± 01	15·615 ± 02	15·587	15·594	15·586	15·566
$^{208}Pb/^{204}Pb$	38·653 ± 10	38·547 ± 04	38·685 ± 11	38·610 ± 09	38·417 ± 08	38·555 ± 03	38·671 ± 05	38·579	38·668	38·629	38·483
Modal composition (vol. %)											
olivine	—	—	—	—	17	14	5	3	4	15	12
orthopyroxene	6	7	3	8	—	—	—	—	2	—	—
clinopyroxene	5	6	2	7	5	4	8	1	—	2	1
plagioclase	17	16	15	15	—	—	20	—	—	—	—
groundmass	72	71	80	70	78	82	67	96	94	83	87
K (wt %)	2·35 ± 0·05	2·02 ± 0·04	2·50 ± 0·05	1·77 ± 0·04	1·17 ± 0·02	1·14 ± 0·02	1·15 ± 0·02				
^{36}Ar (10^{-8} cm^3 STP/g)	0·222 ± 0·004	0·326 ± 0·006	1·036 ± 0·016	0·231 ± 0·003	0·309 ± 0·015	0·635 ± 0·010	0·039 ± 0·003				
$^{40}Ar/^{36}Ar$	820·45 ± 16·62	638·53 ± 13·36	399·57 ± 7·05	714·78 ± 11·88	492·82 ± 13·86	370·45 ± 6·42	510·80 ± 44·92				
Rad. ^{40}Ar (10^{-8} cm^3 STP/g)	116·4 ± 1·9	111·8 ± 2·4	107·8 ± 4·9	97·05 ± 1·61	60·96 ± 4·43	47·61 ± 2·76	8·418 ± 0·717				
Air cont. (%)	36·0	46·3	74·0	41·3	60·0	79·8	57·9				
Age (Ma)	12·7 ± 0·3	14·2 ± 0·4	11·1 ± 0·6	14 ± 0·4	13·3 ± 0·5	10·7 ± 0·3	1·88 ± 0·16				

*Total iron as Fe_2O_3.
[1]Plagioclase-phyric andesite.
[2]High-magnesium andesite.
[3]Representative HMA and basalt from the SVB (Tatsumi & Ishizaka, 1982; Shimoda *et al.*, 1998).
[4]Corrected for K–Ar ages obtained as part of this study.

Table 2: Representative composition of olivine phenocrysts in HMAs

Sample:	OT-S	OT-S	OT-S	OT-6.2	OT-6.2	OT-6.2
Position:	core	core	core	core	core	core
SiO_2	40·95	40·41	39·55	39·25	38·81	38·50
FeO*	9·32	11·54	13·88	14·21	18·45	22·38
MnO	0·14	0·17	0·21	0·22	0·29	0·36
MgO	49·85	48·36	46·37	45·63	41·83	39·41
CaO	0·11	0·10	0·11	0·11	0·14	0·16
NiO	0·40	0·27	0·14	0·38	0·27	0·17
Total	100·78	100·86	100·26	99·80	99·77	100·97
Si	0·995	0·991	0·987	0·987	0·995	0·993
Fe	0·189	0·237	0·290	0·299	0·395	0·483
Mn	0·003	0·004	0·004	0·005	0·006	0·008
Mg	1·806	1·768	1·726	1·711	1·598	1·515
Ca	0·003	0·003	0·003	0·003	0·004	0·004
Ni	0·008	0·005	0·003	0·008	0·005	0·003
Total	3·004	3·008	3·012	3·012	3·004	3·006
O	4·000	4·000	4·000	4·000	4·000	4·000
Mg/(Mg + Fe)	0·905	0·882	0·856	0·851	0·802	0·758

*Total iron as FeO.

OT-6.2 is higher than that in HMA OT-S (Fig. 4c). Olivine phenocrysts in both HMAs commonly contain chromite inclusions. In HMA OT-S these chromites show limited compositional variation, whereas those in HMA OT-6.2 range from chromite to chromian titanomagnetite (Fig. 5).

Plagioclase-phyric andesites (PAs) of Miocene age display disequilibrium petrographic features such as the occurrence of reversely zoned plagioclase and pyroxene phenocrysts (Tables 5 and 6), a feature commonly observed in calc-alkalic andesites (e.g. Sakuyama, 1979).

The compositions of the Miocene andesites plot within the broad calc-alkalic trend of the Setouchi volcanic rocks, whereas the Quaternary andesite TO-2.2 exhibits characteristics different from those of the SVB lavas (Fig. 6). HMAs and PAs in NE Kyushu have major and trace element compositions and normal-type mid-ocean ridge basalt (N-MORB)-normalized incompatible element patterns identical to those in the other regions of the SVB (Figs 6 and 7), which typify both subduction zone magmas and continental crust compositions; i.e. higher concentrations of elements with higher incompatibility during mantle melting with relative depletion and enrichment in Nb and Pb, respectively. However, NE Kyushu PAs are distinct from other Setouchi PAs in having higher concentrations of TiO_2 (Fig. 6).

Previous Sr–Nd–Pb isotopic data for the Setouchi volcanic rocks in NE Shikoku (Shimoda *et al.*, 1998; Tatsumi *et al.*, 2002) demonstrated that the PAs have relatively enriched isotopic signatures compared with the HMAs; this is also observed for andesites from NE Kyushu (Fig. 8). On the other hand, the Quaternary andesite TO-2.2 has a more depleted Sr–Nd isotopic signature than the Setouchi rocks, whereas the Pb isotopic composition of the Quaternary andesite is indistinguishable from that of the Setouchi porphyritic andesites (Fig. 8).

Microscopic observation shows that the olivine phenocrysts in HMA OT-6.2 are highly altered and replaced by serpentine/chlorite and unidentifiable clay minerals. A rather low total of major oxides (96·47 wt %) in the bulk-rock analysis is consistent with such alteration. However, it is suggested that the bulk chemical compositions of this particular sample have not been affected significantly by alteration processes, because OT-S and OT-6.2 have similar compositions (Figs 6–8).

DISCUSSION

Setouchi magmatism in NE Kyushu

The K–Ar ages and petrological and geochemical characteristics of the volcanic rocks from the NE

Table 3: Representative composition of spinel inclusions in HMAs

Sample:	OT-S	OT-S	OT-S	OT-6.2	OT-6.2	OT-6.2
SiO_2	0·12	0·11	0·14	0·07	0·10	0·07
TiO_2	0·70	0·70	0·93	0·68	0·74	3·55
Al_2O_3	13·95	12·90	12·36	9·14	8·97	6·80
Cr_2O_3	48·86	50·42	47·49	46·22	38·96	22·05
FeO*	22·16	24·02	29·20	35·21	42·75	59·01
MnO	0·20	0·22	0·25	0·38	0·43	0·35
MgO	12·33	10·64	8·24	5·56	3·45	2·58
CaO	0·05	0·03	0·02	0·06	0·06	0·05
Total	98·37	99·03	98·61	97·32	95·47	94·46
Si	0·004	0·004	0·005	0·002	0·004	0·003
Ti	0·018	0·018	0·024	0·019	0·021	0·110
Al	0·543	0·506	0·499	0·391	0·404	0·330
Cr	1·276	1·328	1·286	1·326	1·177	0·717
Fe[1]	0·612	0·670	0·837	1·068	1·366	2·031
Mn	0·006	0·006	0·007	0·012	0·014	0·012
Mg	0·607	0·528	0·421	0·301	0·197	0·158
Ca	0·002	0·001	0·001	0·002	0·002	0·002
Total	3·069	3·061	3·079	3·121	3·184	3·364
O	4·000	4·000	4·000	4·000	4·000	4·000
Cr/(Cr + Al)	0·701	0·724	0·721	0·772	0·744	0·685
Mg/(Mg + Fe)	0·586	0·511	0·402	0·287	0·184	0·130
$Cr/(Cr + Al + Fe^{3+})$	0·637	0·665	0·645	0·650	0·568	0·356
$Al/(Cr + Al + Fe^{3+})$	0·271	0·253	0·250	0·192	0·195	0·164
$Fe^{3+}/(Cr + Al + Fe^{3+})$	0·091	0·082	0·105	0·158	0·237	0·481
Olivine[2]	0·894	0·866	0·850	0·826	0·791	0·764

*Total iron as FeO.
[1]Total iron as Fe^{2+}; Fe^{3+} is calculated assuming stoichiometry for spinel.
[2]Mg/(Mg + Fe) of coexisting olivine.

Kyushu region confirm previous suggestions that Setouchi magmatism also occurred in this region (e.g. Tatsumi, 1983). The reasons for this are twofold. First, the magmatism in this region is almost synchronous with that in other regions of the SVB (Fig. 3). Second, both HMAs and PAs in this region yield middle Miocene K–Ar ages and have geochemical characteristics identical to, or close to, those of Setouchi lavas in other regions (Figs 6–8). On the other hand, the Quaternary andesite TO-2.2 has a major and trace element and Sr–Nd–Pb isotopic signature different from that of the other Setouchi volcanic rocks (Figs 6 and 9).

The occurrence of plagioclase-free, rather aphyric andesites (sanukitoids), which typify Setouchi magmatism, has been reported from the western and central part of Kyushu (e.g. Shiraki *et al.*, 1995). These rocks, however, have K–Ar ages younger than and/or geochemical characteristics different from those of the Setouchi lavas (Tatsumi *et al.*, 1980; Shiraki *et al.*, 1995). This, together with the results of this study, suggests that the Setouchi magmatism occurred only during a specific time window from 11 to 16 Ma and that the NE Kyushu region is the western tip of the SVB.

To the south of the SW Japan arc is the Shikoku Basin, a back-arc basin created behind the Izu–Bonin–Mariana arc between 26 and 15 Ma (Okino *et al.*, 1994), immediately before the Setouchi magmatism began. It is thus intuitively expected that the unusual subduction of such a young oceanic plate beneath the Setouchi region could cause magmatism in the SVB that is characterized by the occurrence of unusual HMAs (Tatsumi & Maruyama, 1989). Furukawa & Tatsumi (1999) demonstrated, on the basis of numerical simulations, that the temperature of the surface of the young Shikoku Basin lithosphere was high enough to allow partial melting during subduction. The location of the western tip of the SVB in the NE Kyushu

Table 4: Representative composition of clinopyroxene phenocrysts in HMAs

Sample:	OT-S	OT-S	OT-S	OT-6.2	OT-6.2	OT-6.2
Position:	core	core	core	core	core	core
SiO_2	53·55	52·30	49·62	53·48	51·83	51·26
TiO_2	0·28	0·30	1·36	0·29	0·56	0·99
Al_2O_3	1·64	2·39	6·33	2·26	2·80	4·26
Cr_2O_3	0·86	1·09	0·12	0·82	0·53	0·36
FeO*	4·30	4·75	6·91	4·35	5·36	7·47
MnO	0·14	0·14	0·19	0·13	0·16	0·19
MgO	18·29	17·59	15·26	17·90	16·46	17·34
CaO	21·08	20·58	19·92	20·84	21·61	17·99
Na_2O	0·28	0·27	0·36	0·30	0·26	0·39
Total	100·44	99·41	100·07	100·36	99·57	100·25
Si	1·944	1·923	1·826	1·939	1·912	1·876
Ti	0·008	0·008	0·038	0·008	0·015	0·027
Al	0·070	0·103	0·274	0·096	0·122	0·184
Cr	0·025	0·032	0·004	0·024	0·015	0·010
Fe	0·131	0·146	0·213	0·132	0·165	0·229
Mn	0·004	0·004	0·006	0·004	0·005	0·006
Mg	0·990	0·964	0·837	0·968	0·905	0·946
Ca	0·820	0·811	0·786	0·810	0·854	0·706
Na	0·020	0·019	0·026	0·021	0·019	0·028
Total	4·011	4·011	4·009	4·002	4·013	4·012
O	6·000	6·000	6·000	6·000	6·000	6·000
Mg/(Mg + Fe)	0·883	0·868	0·797	0·880	0·845	0·805

*Total iron as FeO.

region may be consistent with such a process, including partial melting of associated sediments. The Kyushu–Palau ridge, which forms the western margin of the Shikoku Basin, has been subducted beneath Kyushu (Fig. 1). In other words, a hot lithosphere capable of partial melting at ~11–15 Ma was being subducted beneath NE Kyushu, but not beneath Central to West Kyushu.

Origin of SVB magmas in NE Kyushu

Experimental results suggest that hydrous melting of peridotite is a possible mechanism for andesite magma generation in the upper mantle (e.g. Kushiro, 1969; Hirose, 1997). However, such results do not necessarily imply the direct addition of slab-derived aqueous fluids to the mantle wedge. Most researchers have favoured a mechanism for HMA magma production including partial melting of the subducting oceanic lithosphere and interaction of these slab-derived, hydrous, silicic melts with the overlying mantle peridotites in the mantle wedge (Kay, 1978; Pearce *et al.*, 1992; Yogodzinski *et al.*, 1994; Kelemen, 1995). As for the Setouchi HMAs, Shimoda *et al.* (1998) demonstrated that the Pb, Sr, and Nd isotopic compositions of such HMAs overlap those of the subducting local terrigenous sediments and may be explained by a contribution of partial melts derived from such sediments, rather than aqueous fluids from the dehydrating slab. Furthermore, Tatsumi (2001) examined this process based on a geochemical formulation of partial melting and melt–solid reactions, and demonstrated that a melt, produced by partial melting of subducted sediment at 1050°C and 1·0 GPa, changes its composition from rhyolitic to andesitic as olivine and clinopyroxene dissolve and orthopyroxene crystallizes. The resulting reaction product has major and incompatible trace element characteristics close to those of the HMAs in the SVB. It should be stressed that such processes, including melting of subducted sediments, are supported by numerical simulations of temperature distribution along the surface of the subducting Shikoku Basin lithosphere (Furukawa & Tatsumi, 1999).

NE Kyushu HMAs, as well as those in the other regions of the SVB, are suggested to be mantle-derived magmas because of (1) their high MgO/FeO ratios and

Table 5: Representative composition of reversely zoned plagioclase phenocrysts in PAs

Sample:	OT-1	OT-1	OT-3	OT-3
Position:	core	rim	core	rim
SiO_2	53·54	52·26	50·20	48·59
TiO_2	0·05	0·01	0·08	0·01
Al_2O_3	28·41	29·56	30·23	32·05
FeO*	0·20	0·24	0·49	0·29
MnO	0·00	0·00	0·04	0·04
MgO	0·12	0·08	0·48	0·06
CaO	12·36	13·39	15·09	16·30
Na_2O	4·35	3·77	2·98	2·15
K_2O	0·31	0·27	0·17	0·12
Total	99·32	99·58	99·74	99·60
Si	2·442	2·385	2·304	2·236
Ti	0·002	0·000	0·003	0·000
Al	1·527	1·590	1·635	1·738
Fe	0·007	0·009	0·019	0·011
Mn	0·000	0·000	0·002	0·001
Mg	0·008	0·005	0·033	0·004
Ca	0·604	0·655	0·742	0·804
Na	0·384	0·334	0·265	0·191
K	0·018	0·015	0·010	0·007
Total	4·992	4·993	5·011	4·993
O	8·000	8·000	8·000	8·000
Ca/(Ca + Na)	0·611	0·662	0·737	0·808

*Total iron as FeO.

Table 6: Representative composition of reversely zoned orthopyroxene phenocrysts in PAs

Sample:	OT-1	OT-1	OT-3	OT-3
Position:	core	rim	core	rim
SiO_2	54·27	55·16	54·85	55·78
TiO_2	0·49	0·30	0·40	0·35
Al_2O_3	0·90	0·87	0·78	0·88
Cr_2O_3	0·06	0·06	0·07	0·03
FeO*	16·55	15·13	16·20	15·67
MnO	0·34	0·36	0·35	0·32
MgO	25·39	26·42	25·25	26·42
CaO	1·95	1·81	1·95	1·90
Na_2O	0·03	0·02	0·03	0·03
Total	99·97	100·12	99·87	101·37
Si	1·973	1·985	1·990	1·986
Ti	0·013	0·008	0·011	0·009
Al	0·039	0·037	0·033	0·037
Cr	0·002	0·002	0·002	0·001
Fe	0·503	0·455	0·492	0·467
Mn	0·010	0·011	0·011	0·010
Mg	1·376	1·417	1·366	1·403
Ca	0·076	0·070	0·076	0·072
Na	0·002	0·001	0·002	0·002
Total	3·993	3·986	3·982	3·987
O	6·000	6·000	6·000	6·000
Mg/(Mg + Fe)	0·732	0·757	0·735	0·750

*Total iron as FeO.

Ni contents equivalent to those in melts in equilibrium with mantle olivine, and (2) the presence of Mg-rich and Ni-rich olivine phenocrysts (e.g. Tatsumi, 1981, 1982). Furthermore, HMAs in the NE Kyushu region have incompatible trace element characteristics identical to those of HMAs in other regions of the SVB (Fig. 7), providing compelling evidence to suggest that the NE Kyushu HMA magmas are also produced by interaction of slab-sediment melt with mantle wedge peridotites.

HMAs in the NE Kyushu region are distinct among those in the SVB in that they have relatively enriched Sr–Nd and relatively depleted Pb isotopic signatures (Fig. 8). A possible explanation for such 'inconsistent' isotopic signatures may be compositional diversity in the subducting sediments. Evidence for this is twofold. First, subducting sediments are considered to play a key role in the production of HMA magmas through sediment melting and subsequent melt–mantle interaction (Shimoda *et al*., 1998; Tatsumi, 2001). Second, terrigenous and pelitic sediments recovered from the Shikoku Basin have highly variable Sr–Nd–Pb isotopic compositions (Fig. 8).

As is the case in other regions of the SVB, the PAs in NE Kyushu have more enriched Sr–Nd–Pb isotopic signatures than the HMAs (Fig. 8). The PAs in the SVB are distinct from the HMAs because of the presence of reversely zoned plagioclase and pyroxene phenocrysts. Tatsumi *et al*. (2002) demonstrated that such disequilibrium petrographic features in the PAs in the NE Shikoku region can be best explained by mixing of compositionally different magmas such as basalt, two types of HMAs, evolved andesite, and rhyolite. Although it is difficult, because of limited data on the phenocryst compositions in the PA samples studied here, to identify the end-member magmas, mixing of magmas could play a key role in the production of the NE Kyushu PAs displaying such disequilibrium petrographic features. If so, then HMA and rhyolitic magmas, both occurring in this region, could be candidates for end-member magmas. As rhyolites possess relatively enriched isotopic signatures compared with

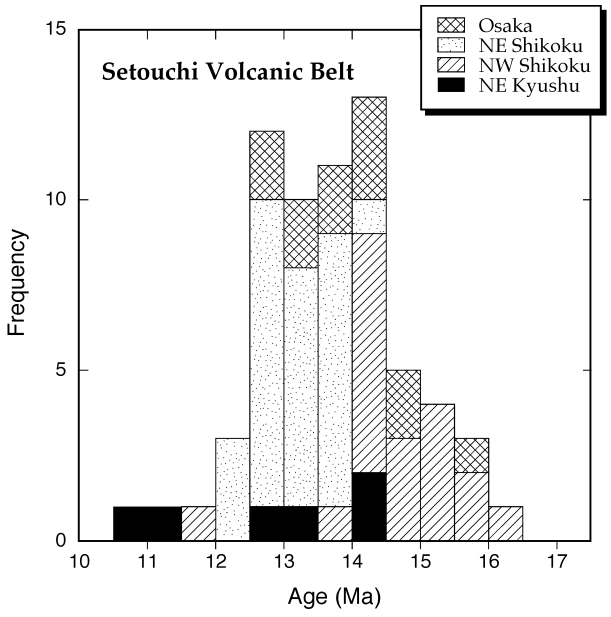

Fig. 3. Frequency distribution diagram for K–Ar ages of the Setouchi volcanic rocks. The magmatism in the NE Kyushu region is almost synchronous with that in other regions of the SVB.

other rocks in the SVB (Fig. 8), the isotopic characteristics of PAs in the NE Kyushu region may be explained by the involvement of rhyolitic magmas in the production of the PA magmas. However, NE Kyushu PAs have more enriched Sr–Nd isotopic compositions than the rhyolites in the other regions of the SVB (Fig. 8). It should be stressed that the basement rocks in the SVB are also characterized by enriched isotopic signatures (Fig. 8), suggesting that crustal contamination may be an additional process in the petrogenesis of the more evolved and isotopically enriched PAs (Tatsumi *et al.*, 2002).

Variations in the magma source compositions

The geochemical characteristics of the pre-subduction modification mantle source cannot be estimated solely based on the isotopic compositions of the magmas, because of the variable contributions of different metasomatic agents to the magma source. However, the following petrographic observations may provide insights into the characteristics of the magma sources or melting residues beneath the NE Kyushu region. The HMA OT-S sample contains olivine phenocrysts characterized by high NiO contents (up to 0·45 wt %) and Mg/(Mg + Fe) ratios (up to 0·91) (Fig. 4c), which are the most Ni- and Mg-rich olivines reported from the SVB (Tatsumi *et al.*, 2002). Two types of HMAs are recognized in the SVB (Tatsumi, 1982): one with the crystallization sequence of olivine → orthopyroxene (opx-HMA) and the other with olivine → clinopyroxene (cpx-HMA). The results of high-pressure melting experiments (Tatsumi, 1981, 1982) indicate that harzburgitic and lherzolitic peridotites are the melting residues for opx- and cpx-HMA magmas, respectively. The results led Tatsumi (1982) to the conclusion that the opx-HMA magmas are produced by higher degrees of partial melting or from relatively depleted mantle peridotite source compared with the cpx-HMA magmas. This is consistent with the difference in olivine compositions, specifically higher NiO and Mg/(Mg + Fe) for the opx-HMA magmas (Fig. 4c). Although the HMAs in the NE Kyushu region are classified in terms of their phenocryst assemblage as cpx-HMAs, their olivine phenocrysts have compositions identical to those in opx-HMAs (Fig. 4c) and are indicative of derivation of these magmas from a depleted mantle source.

Chromian spinel often co-precipitates with olivine in Mg-rich, primitive magmas. Although the behaviour of Cr in chromian spinel is complex, depending on pressure (e.g. Dick & Bullen, 1984), oxygen fugacity (e.g. Murck & Campbell, 1986), temperature (e.g. Murk & Campbell, 1986), and magma chemistry (Allan *et al.*, 1988), Cr/(Cr + Al) ratios have been often used to determine magma–restite genetic linkages (e.g. Dick & Bullen, 1984). Arai (1994) examined the characteristics of mantle restites for Mg-rich magmas, based on the compositional relations between Cr/(Cr + Al) ratios in chromian spinel inclusions and Mg/(Mg + Fe) ratios in the host olivine phenocrysts, and proposed the olivine–spinel mantle array (Fig. 5f) as a possible compositional variation trend for the compositions of olivine and spinel in the mantle. He further indicated that HMAs in the SVB and boninites are derived from mantle peridotites more depleted, in terms of Cr/(Cr + Al) ratios in spinel, than other magma types such as basalts from NE Japan (Fig. 5f). It is suggested that opx-HMAs in the SVB possess significantly depleted olivine–spinel compositional signatures compared with the cpx-HMAs (Fig. 5f). This can be explained by opx-HMA magma generation by greater degrees of partial melting or from more depleted sources than the cpx-HMA magmas. The olivine–spinel compositional relations for HMAs in the NE Kyushu region (Fig. 5f) may also suggest that they are derived from spinel peridotites more depleted, in terms of their spinel compositions, than other cpx-HMA magmas in the SVB, which is consistent with the above-mentioned discussion based on the NiO–Mg/(Mg + Fe) relation for olivine phenocrysts.

The chemical compositions of partial melts produced from compositionally variable peridotites have been investigated at high pressures (e.g. Falloon *et al.*,

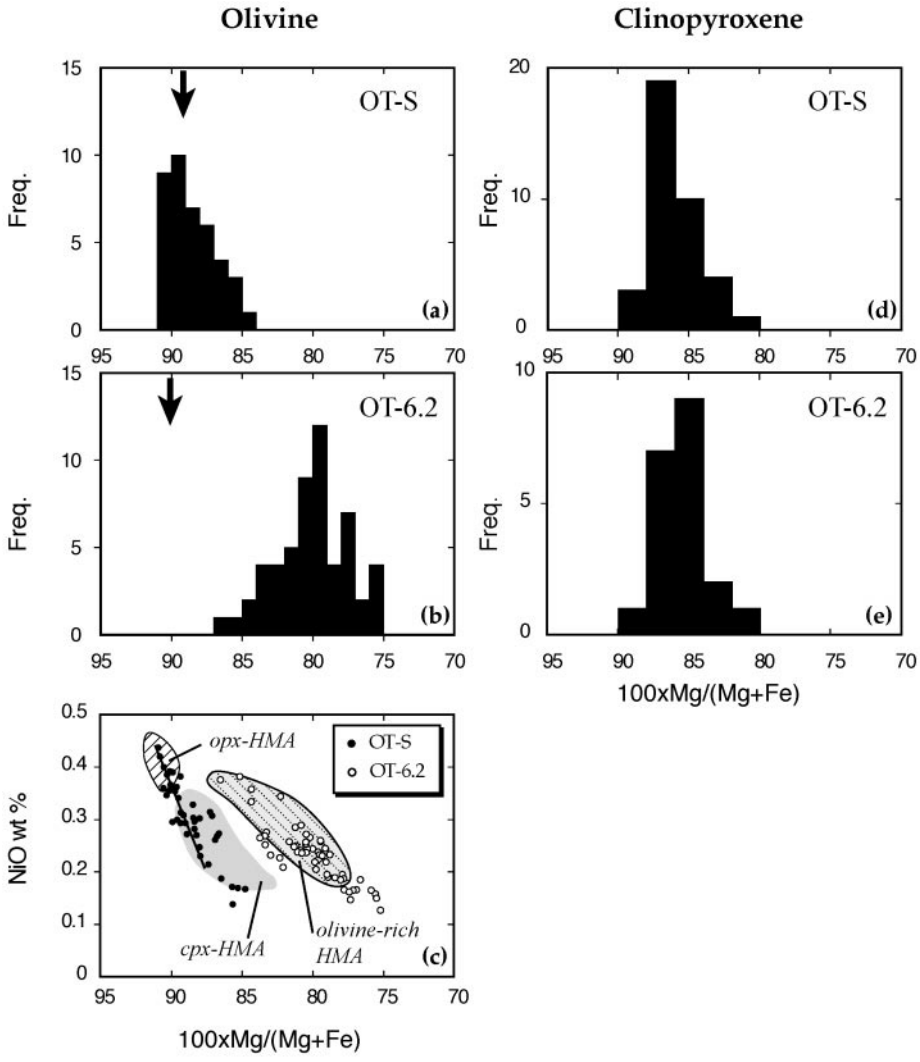

Fig. 4. Compositions of olivine (a–c) and clinopyroxene (d and e) phenocrysts in HMAs OT-S and OT-6.2. Arrows indicate compositions of olivine in equilibrium with the host rock, calculated based on the Fe–Mg exchange partitioning and an inferred Fe^{3+}/Fe^{2+} ratio in the magma. An olivine perfect fractionation trend is also shown by the continuous line in (c) (see text). Olivine phenocrysts in HMA OT-6.2, as well as those in olivine-rich HMAs from other regions of the SVB, possess compositions in disequilibrium with the magma.

1988; Hirose & Kushiro, 1993; Baker & Stolper, 1994). It has been established (e.g. Kushiro, 2001), based on these experimental results, that the FeO content of the partial melts depends on the degree of depletion of the source, as evidenced by its Mg/(Mg + Fe) ratio (Fig. 9). Although such relations have not been examined systematically under hydrous conditions, opx-HMAs may be derived from a more depleted mantle source or produced by higher degrees of partial melting than cpx-HMAs. Although spinel and olivine compositions in the studied HMAs from the NE Kyushu region possess characteristics similar to those for opx-HMAs in the SVB (Fig. 5a and f), they have higher FeO* contents at a given MgO than other HMAs in the SVB (Fig. 9). It may be thus suggested that the NE Kyushu HMAs are generated by higher degrees of partial melting of a peridotite source with an original composition similar to that for cpx-HMAs in other regions of the SVB.

Two types of HMAs with different rates of cooling

Although both HMAs, OT-6.2 and OT-S, possess similar bulk-rock (i.e. volatile-free) chemical compositions, the olivine phenocrysts and spinel inclusions in these samples exhibit marked compositional differences (Figs 4 and 5). One such difference is that olivine

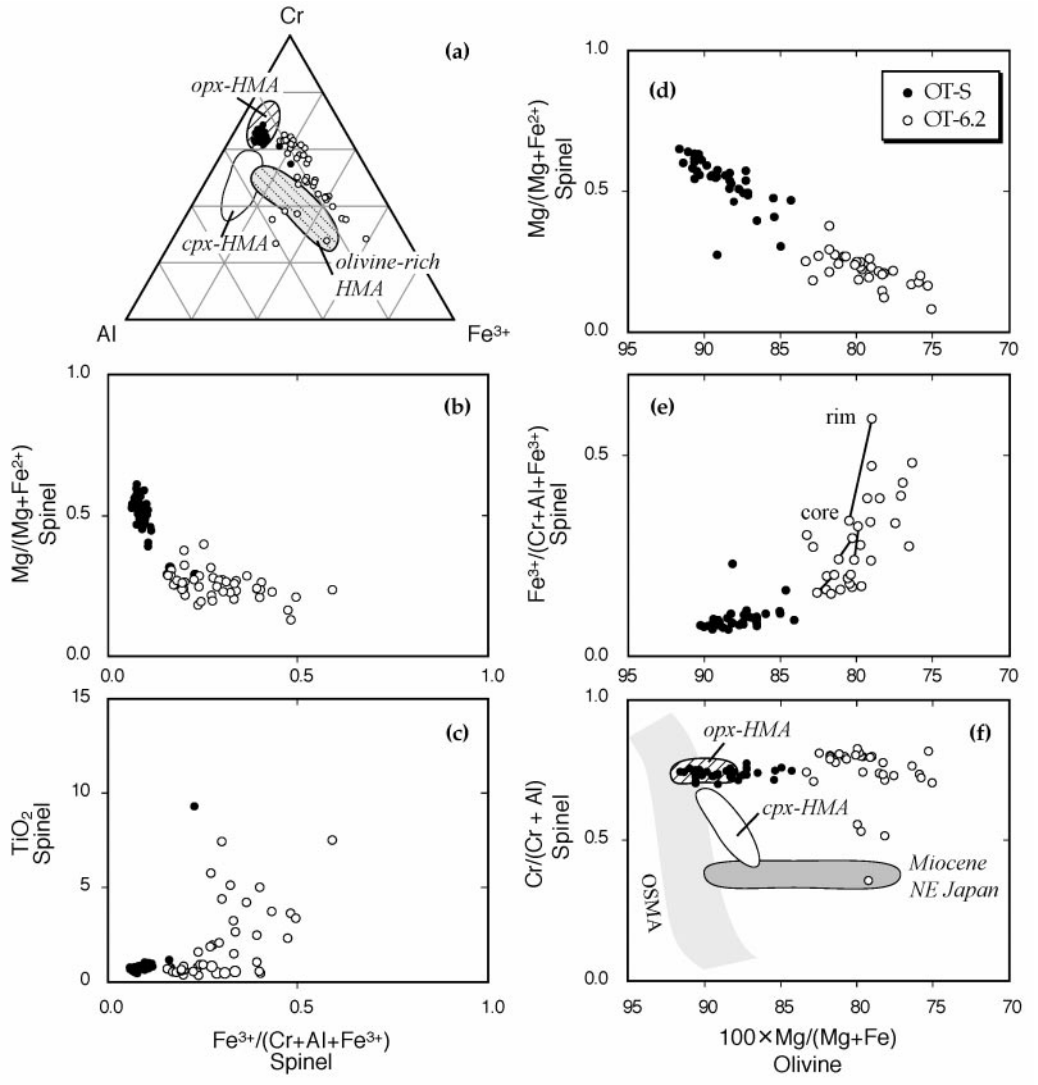

Fig. 5. Compositions of spinel inclusions in olivine phenocrysts (a–c) and spinel–olivine compositional relations (d–f) in HMAs OT-S, OT-6.2 and other regions in the SVB. Spinels included in a single olivine crystal are tie-lined in (e). The unusual Fe^{3+}-rich compositional trend for spinels in HMA-6.2 can be explained by effective elemental diffusion through the olivine crystals associated with the long residence time and the slow rate of cooling of the magmas (see text). Data for cpx-, opx- and olivine-rich HMAs are from Tatsumi & Ishizaka (1981, 1982). OSMA, olivine–spinel mantle array (Arai, 1994).

phenocrysts in OT-6.2 have higher Mg/(Mg + Fe) ratios at a given NiO content than those in OT-S (Fig. 4c). The compositions of olivine in HMA OT-S, which are similar to those in phenocryst-poor (<10%), cpx- and opx-HMAs in the SVB (Fig. 4c), are examined assuming maximum fractionation of olivine from a magma and data for Mg–Fe–Ni partitioning between olivine and liquid. It has been experimentally shown that the $K_D(Fe/Mg)^{ol/liq}$ value depends on pressure, temperature, and melt composition (e.g. Takahashi, 1986; Baker & Stolper, 1994). However, here a constant value of 0·3 (Roeder & Emslie, 1970) was assumed, simply because of the relatively minor effect of such parameters on $K_D(Fe/Mg)^{ol/liq}$ (0·29–0·31). The partition coefficients for Ni, between olivine and liquid of Kinzler *et al.* (1990) were used. A series of magma and olivine compositions were calculated based on a Mg- and Ni-rich olivine phenocryst composition (Mg-number 91, NiO 0·42 wt %) and 1 wt % interval of olivine fractionation at a constant $Fe^{2+}/(Fe^{2+} + Fe^{3+})$ ratio in the magma (0·9). The results of such calculations are shown in Fig. 4c, and suggest that the compositional trend of OT-S olivine can be explained by simple olivine fractionation. It thus follows that some additional mechanisms are needed to understand the origin of the compositional

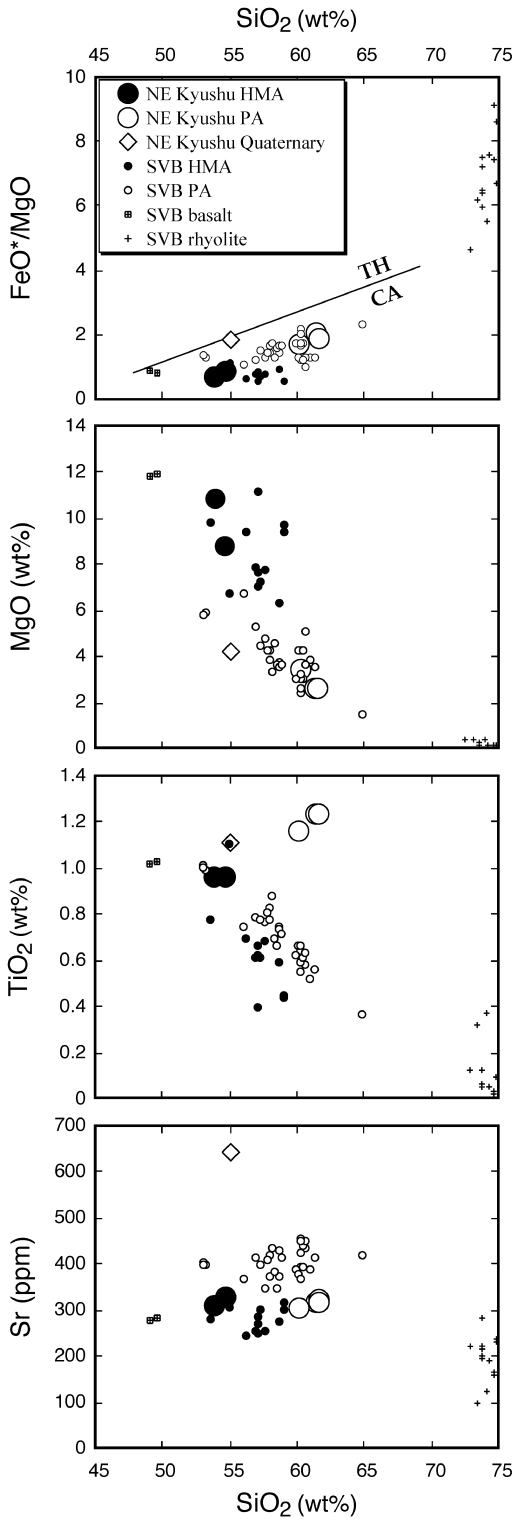

Fig. 6. Variation diagrams for the Quaternary volcanic rock and the Setouchi volcanic rocks from the NE Kyushu region, together with the compositional range for lavas in the SVB (Shimoda *et al.*, 1998; Tatsumi *et al.*, 2002). The Quaternary sample shows characteristics different from those for Setouchi volcanic rocks in NE Kyushu and other regions. TH, tholeiitic rock series; CA, calc-alkalic rock series.

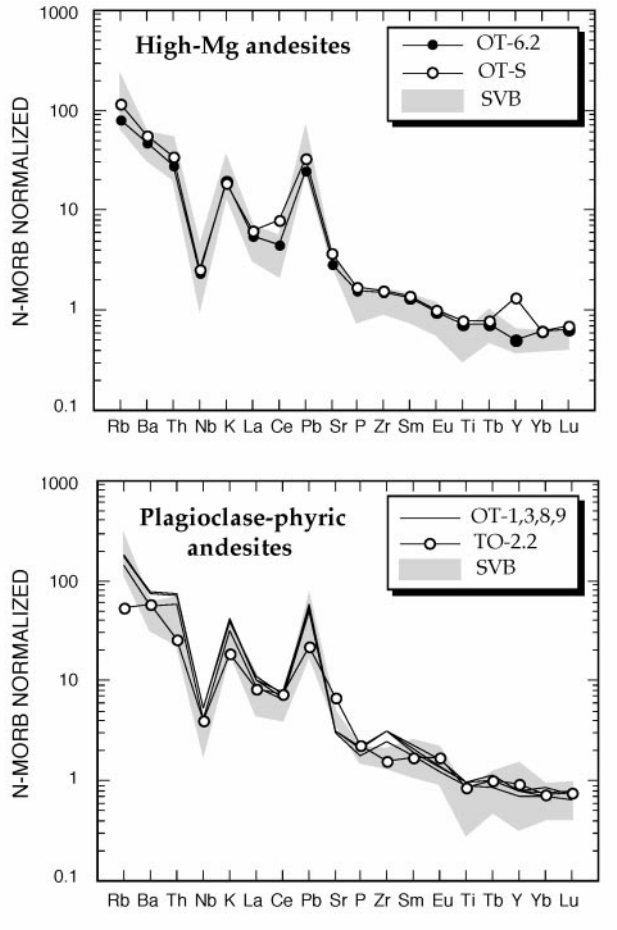

Fig. 7. N-MORB-normalized multi-element diagrams for HMAs and plagioclase-phyric andesites in the SVB (shaded). Miocene volcanic rocks in NE Kyushu region have trace element signatures identical to those for Setouchi lavas in other regions.

trends of olivine for OT-6.2 and for phenocryst-rich (>10%) HMAs in the SVB (Fig. 4c), provided we do not accept the presence of anomalous, Fe-rich olivine in the mantle. Olivine phenocrysts, which have unusually high Ni contents at a given Mg-number, are commonly found in basalts and andesites (e.g. Sato & Banno, 1983; Nabelek & Langmuir, 1986; Nakamura, 1995; Tatsumi *et al.*, 2002). Nakamura (1995) examined the compositional zoning of olivine phenocrysts in calc-alkalic andesites from the Yatsugatake volcano, Central Japan, using a growth and diffusion model in the Mg–Fe–Ni system. He demonstrated that the characteristic, Ni-rich compositions of the olivine phenocrysts can be explained by diffusion processes within normally zoned olivines causing Fe enrichment without a marked depression in the Ni content. This is due to a greater Fe–Mg interdiffusion coefficient than the Ni tracer diffusion coefficient in olivine. It is thus concluded that the long residence time of olivine

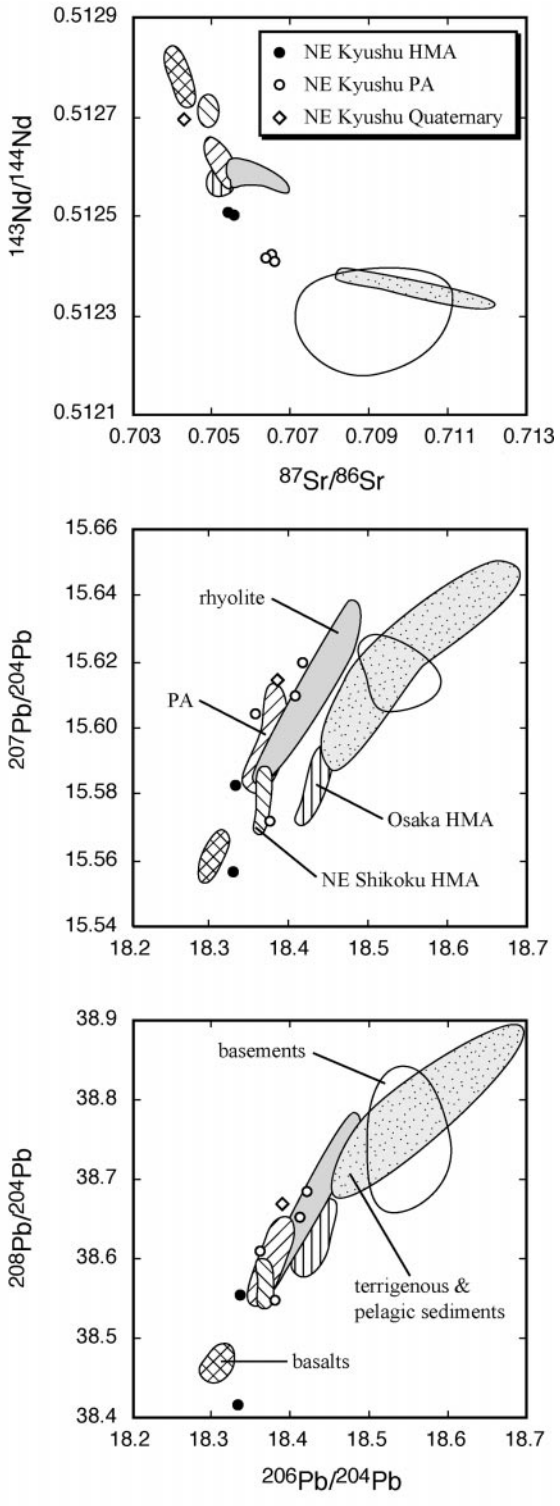

Fig. 8. Sr–Nd–Pb isotopic compositions of Setouchi volcanic rocks, terrigenous sediments from the Nankai Trough, and basement rocks in NE Kyushu and other regions. The Quaternary andesite TO-2.2 has a more depleted Sr–Nd isotopic signature than other lavas from the SVB. Plagioclase-phyric andesites have more enriched Sr–Nd–Pb isotopic characteristics than HMAs in NE Kyushu, as well as other regions of the SVB (Shimoda *et al.*, 1998; Tatsumi *et al.*, 2002).

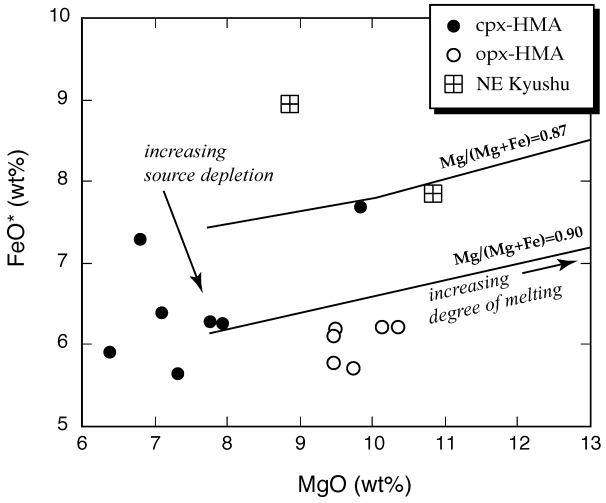

Fig. 9. MgO–FeO relations for Setouchi HMAs [data from this study and Shimoda *et al.* (1998)] and partial melts formed from two peridotites having different Mg/(Mg + Fe) ratios at 1·0 GPa (Kushiro, 2001). It is suggested that opx-HMA magmas are produced by higher degrees of partial melting or derived from more depleted peridotites than cpx-HMAs.

phenocrysts in a magma chamber may cause such Ni- and Fe-rich compositions. The presence of anomalously nickeliferous olivine in HMA OT-6.2 could also be explained by this mechanism. The observation that the Setouchi HMAs enriched in olivine phenocrysts distinctively contain such nickeliferous olivines (Fig. 4c) may also be consistent with the long residence time of the magmas rather than a simple olivine fractionation process in an HMA magma.

It has been suggested that the chemistry of chromian spinel is also dependent on the cooling rate, even if the magma chemistry is the same (e.g. Ozawa, 1984). Scowen *et al.* (1991) documented the chemical variability of chromian spinel included in olivine phenocrysts in the 1959 Kilauea Iki lava lake: liquidus chromian spinel compositions are preserved only in scoria that was rapidly quenched from eruption temperatures, whereas samples from the lava lake show that chromian spinel is richer in Fe^{2+}, Fe^{3+}, Ti and poorer in Mg, Al, Cr compared with the liquidus spinel. It is further documented that the degree of such a compositional shift depends on the time elapsed since the last eruption, the cooling history of the sample, the extent of differentiation of the interstitial melt, and the position of the spinel inclusion within a single olivine phenocryst. These observations led Scowen *et al.* (1991) to the conclusion that the compositional changes in the chromian spinel inclusions may be caused by re-equilibration with the residual melt by cationic diffusion (Mg, Al and Cr outwards, and Fe^{2+}, Fe^{3+} and Ti inwards) through the olivine crystals. This mechanism may also explain the following

compositional differences and changes of chromian spinel inclusions in HMAs OT-6.2 and OT-S (Fig. 5), which are almost identical to those in Kilauea Iki samples: (1) chromian spinels in HMA OT-6.2 are enriched in Fe^{2+}, Fe^{3+} and Ti, and depleted in Mg, Al and Cr compared with those in HMA OT-S (Fig. 5a–c); (2) such compositional differences are also observed for chromian spinels included in a single olivine phenocryst in HMA OT-6.2 as a function of the distance from the rim of an olivine crystal (Fig. 5e). These characteristic compositional changes are also observed for spinel inclusions in the Setouchi HMAs with a great proportion of phenocrysts (Fig. 5a). It may thus be suggested that the composition of the chromian spinel inclusions, as well as those of the olivine phenocrysts, may indicate a longer residence time of the magma and a slower cooling rate for HMA OT-6.2 than for HMA OT-S.

Alternatively, the unusually Ni- and Fe-rich olivine compositions might be caused by disequilibrium crystallization during supercooling. Tamura *et al.* (2000) demonstrated the presence of two types of olivine phenocrysts in basalts from the Daisen volcano, SW Japan; one exhibiting compositions more enriched in both Ni and Fe than the other. Such Ni-, Fe-rich olivines are not in equilibrium with the host magma in terms of Mg–Fe–Ni exchange partitioning and exhibit characteristic skeletal morphologies. However, the characteristic high $Fe^{3+}/(Al + Cr + Fe^{3+})$ ratios at a rather constant Cr/Al ratio observed for spinel inclusions in HMA OT-6.2 (Fig. 5) cannot be explained solely by such a disequilibrium crystallization process.

CONCLUSION

High-magnesium andesites (HMAs) and plagioclase-phyric andesites (PAs) from NE Kyushu may form the western tip of the Setouchi Volcanic Belt (SVB), which is characterized by HMA magmatism. Evidence for this is twofold. First, K–Ar ages obtained for these andesites are well within the range of those for volcanic rocks in other regions of the SVB, whereas HMAs in Central to West Kyushu formed significantly later than Setouchi magmatism (Tatsumi, 1980; Shiraki *et al.*, 1995). Second, the geochemical characteristics of both HMAs and PAs in NE Kyushu are identical to those of other Setouchi lavas. Setouchi magmatism in the NE Kyushu region, especially the generation of HMA magmas, may have been caused by the subduction of newly formed and hence, hot lithosphere of the Shikoku Basin, as is similarly proposed for Setouchi magmas in other regions. This is consistent with the present-day tectonic setting of Kyushu, where the Kyushu–Palau ridge, forming the western margin of the Shikoku Basin, is currently being subducted beneath Central Kyushu. On the other hand, HMAs, with younger ages than those in the SVB, are also found in Western and Central Kyushu. Such HMAs could not have been produced by a process including partial melting of subducting sediments and subsequent melt–mantle interaction, which has been proposed to explain the generation of the Setouchi HMA magmas, as the Shikoku Basin lithosphere, which was hot enough for partial melting during Setouchi magmatism, was not subducting beneath these regions. The origin of such HMAs may be related to a mantle thermal anomaly caused by back-arc rifting and asthenospheric injection (Shinjo *et al.*, 2000) and must be further examined.

Two types of HMAs, having almost identical bulk chemical compositions but showing different mineralogical characteristics, occur in NE Kyushu. Although one shows petrographic characteristics common to most primitive Setouchi HMAs, the other contains Fe-rich and Ni-rich olivine phenocrysts and Fe^{2+}-, Fe^{3+}-, and Ti-rich chromian spinel inclusions. HMAs that contain such characteristic olivine and spinel are also found elsewhere in the SVB and are distinct in their high modal abundances of olivine phenocrysts. These observations may be explained by the long residence time of the magma and the slow cooling rate of the magma, causing element diffusion within and through the olivine phenocrysts. If so, then special attention must be paid when estimating the characteristics of the residual mantle peridotite by using olivine–spinel compositional relations in basalts, even if chromian spinels are completely surrounded by olivine phenocrysts.

ACKNOWLEDGEMENTS

We thank Keiichi Shiraki and Hayaomi Urano for providing a high-magnesium andesite sample (OT-S), Yoshihiko Tamura and Shoji Arai for constructive discussions, and Miki Fukuda for preparing figures and the manuscript. The manuscript was greatly improved by critical reviews by Simon Johnson, Jun-Ichi Kimura, Jamie Allan, and Richard Arculus.

REFERENCES

Allan, J. F., Sack, R. O. & Batiza, R. (1988). Cr-rich spinels as petrogenetic indicators: MORB-type lavas from the Lamont seamount chain, eastern Pacific. *American Mineralogist* **73**, 741–753.

Arai, S. (1994). Compositional variation of olivine–chromian spinel in Mg-rich magmas as a guide to their residual spinel peridotites. *Journal of Volcanology and Geothermal Research* **59**, 279–293.

Baker, M. B. & Stolper, E. M. (1994). Determining the composition of high-pressure mantle melts using diamond aggregates. *Geochimica et Cosmochimica Acta* **58**, 2811–2827.

Christensen, U. R. & Mooney, W. D. (1995). Seismic velocity structure and composition of the continental crust: a global view. *Journal of Geophysical Research* **100**, 9761–9788.

Crawford, A. J., Falloon, T. J. & Green, D. H. (1989). Classification, petrogenesis and tectonic setting of boninites. In: Crawford, A. J. (ed.) *Boninites*. London: Unwin Hyman, pp. 1–49.

Dick, H. J. B. & Bullen, T. (1984). Chromian spinel as a petrogenetic indicator in abyssal and alpine-type peridotites and spatially associated lavas. *Contributions to Mineralogy and Petrology* **86**, 54–76.

Falloon, T. J., Green, D. H., Hatton, C. J. & Harris, K. L. (1988). Anhydrous partial melting of a fertile and depleted peridotite from 2 to 30 Kb and application to basalt petrogenesis. *Journal of Petrology* **29**, 1257–1282.

Furukawa, Y. & Tatsumi, Y. (1999). Melting of a subducting slab and production of high-Mg andesite magmas; unusual magmatism in SW Japan at 13 approximately 15 Ma. *Geophysical Research Letters* **26**, 2271–2274.

Goto, A. & Tatsumi, Y. (1994). Quantitative analysis of rock samples by an X-ray fluorescence spectrometer (I). *The Rigaku Journal* **11**, 40–59.

Goto, A. & Tatsumi, Y. (1996). Quantitative analysis of rock samples by an X-ray fluorescence spectrometer (II). *The Rigaku Journal* **13**, 20–38.

Hirose, K. (1997). Melting experiments on lherzolite KLB-1 under hydrous conditions and generation of high-magnesian andesitic melts. *Geology* **25**, 42–44.

Hirose, K. & Kushiro, I. (1993). Partial melting of dry peridotites at high pressures; determination of compositions of melts segregated from peridotite using aggregates of diamond. *Earth and Planetary Science Letters* **114**, 477–489.

Jenner, G. A. (1981). Geochemistry of high-Mg andesites from Cape Vogel, Papua New Guinea. *Chemical Geology* **33**, 307–332.

Kamata, H. (1985). Volcanic activity in relation to the geologic structure in central–north Kyushu, Japan. *Report Geological Survey of Japan* **264**, 31–64.

Kay, R. W. (1978). Aleutian magnesian andesites; melts from subducted Pacific Ocean crust. *Journal of Volcanology and Geothermal Research* **4**, 117–132.

Kelemen, P. B. (1995). Genesis of high Mg andesites and the continental crust. *Contributions to Mineralogy and Petrology* **120**, 1–19.

Kinzler, R. J., Grove, T. L. & Recca, S. I. (1990). An experimental study on the effect of temperature and melt composition on the partitioning of nickel between olivine and silicate melt. *Geochimica et Cosmochimica Acta* **54**, 1255–1265.

Kuroda, N., Shiraki, K. & Urano, H. (1978). Boninite as a possible calc-alkalic primary magma. *Bulletin of Volcanology* **41**, 563–575.

Kushiro, I. (1969). The system forsterite–diopside–silica with and without water at high pressures. *American Journal of Science* **267-A**, 269–294.

Kushiro, I. (2001). Partial melting experiments on peridotite and origin of mid-ocean ridge basalt. *Annual Review of Earth and Planetary Sciences* **29**, 71–107.

Masuda, Y., Yagi, S. & Asayama, T. (1974). Instrumental neutron activation analysis of 13 trace elements in volcanic rocks. *Bulletin of the University of Osaka Prefecture, Series A* **23**, 203–213.

Matsumoto, A. (1989). Improvement for determination of potassium in K–Ar dating. *Bulletin of Geological Survey of Japan* **40**, 65–70.

Murck, B. W. & Campbell, I. H. (1986). The effects of temperature, oxygen fugacity and melt composition on the behaviour of chromium in basic and ultrabasic melts. *Geochimica et Cosmochimica Acta* **50**, 1871–1887.

Nabelek, P. & Langmuir, C. H. (1986). The significance of unusual zoning in olivines from FAMOUS area basalt 527-1-1. *Contributions to Mineralogy and Petrology* **93**, 1–8.

Nagao, K., Nishido, H., Itaya, T. & Ogata, K. (1984). K–Ar age determination. *Bulletin of the Hiruzen Research Institute* **9**, 19–38.

Nakamura, M. (1995). Residence time and crystallization history of nickeliferous olivine phenocrysts from the northern Yatsugatake volcanoes, central Japan; application of a growth and diffusion model in the system Mg–Fe–Ni. *Journal of Volcanology and Geothermal Research* **66**, 81–100.

Okino, K., Shimakawa, Y. & Nagaoka, S. (1994). Evolution of the Shikoku Basin. *Journal of Geomagnetism and Geoelectrics* **46**, 463–479.

Ono, K. (1963). *Explanatory Text of the Geological Map of Japan*, scale 1:50 000. Kujuu: Geological Survey of Japan, 124 pp.

Otofuji, Y., Itaya, T. & Matsuda, T. (1991). Rapid rotation of Southwest Japan; palaeomagnetism and K–Ar ages of Miocene volcanic rocks of Southwest Japan. *Geophysical Journal International* **105**, 397–405.

Ozawa, K. (1984). Olivine–spinel geospeedometry; analysis of diffusion-controlled Mg–Fe^{2+} exchange. *Geochimica et Cosmochimica Acta* **48**, 2597–2611.

Pearce, J. A., van der Laan, S. R., Arculus, R. J., Murton, B. J., Ishii, T., Peate, D. W. & Parkinson, I. J. (1992). Boninite and harzburgite from Leg 125 (Bonin–Mariana forearc); a case study of magma genesis during the initial stages of subduction. In: Fryer, P., *et al.* (eds) *Proceedings of the Ocean Drilling Program, Scientific Results, 125*. College Station, TX: Ocean Drilling Program, pp. 623–659.

Roeder, P. L. & Emslie, R. F. (1970). Olivine–liquid equilibrium. *Contributions to Mineralogy and Petrology* **29**, 275–289.

Rudnick, R. L. & Fountain, D. M. (1995). Nature and composition of the continental crust: a lower crustal perspective. *Reviews of Geophysics* **33**, 267–309.

Saito, K. (1989). Challenges to limits—a case for the K–Ar dating. *Journal of the Mining and Materials Processing Institute of Japan* **105**, 1139–1146.

Sakuyama, M. (1979). Evidence of magma mixing; petrological study of Shirouma-Oike calc-alkaline andesite volcano, Japan. *Journal of Volcanology and Geothermal Research* **5**, 179–208.

Sato, H. (1977). Nickel content of basaltic magmas; identification of primary magmas and a measure of the degree of olivine fractionation. *Lithos* **10**, 113–120.

Sato, H. & Banno, S. (1983). NiO–Fo relation of magnesian olivine phenocryst in high-magnesian andesite and associated basalt–andesite–sanukite from Northeast Shikoku, Japan. *Bulletin of the Volcanological Society of Japan* **28**, 141–156.

Scowen, P. A. H., Roeder, P. L. & Helz, R. T. (1991). Reequilibration of chromite within Kilauea Iki lava lake, Hawaii. *Contributions to Mineralogy and Petrology* **107**, 8–20.

Shibata, K. (1978). Contemporaneity of Tertiary granites in the outer zone of Southwest Japan. *Bulletin—Japan, Geological Survey* **29**, 51–54.

Shibata, K. & Ono, K. (1974). K–Ar ages of the Ono volcanic rocks, central Kyushu. *Bulletin—Japan Geological Survey* **25**, 55–58.

Shimada, M., Sumii, T. & Torii, M. (2001). Paleomagnetic directions and K–Ar ages of Setouchi volcanic rocks in Takanawa peninsula: constraints for the timing of the clockwise rotation of Southwest Japan. *Journal of the Geological Society of Japan* **107**, 773–783.

Shimoda, G., Tatsumi, Y., Nohda, S., Ishizaka, K. & Jahn, B. M. (1998). Setouchi high-Mg andesites revisited; geochemical evidence for melting of subducting sediments. *Earth and Planetary Science Letters* **160**, 479–492.

Shinjo, R., Woodhead, J. D. & Hergt, J. M. (2000). Geochemical variation within the northern Ryukyu Arc; magma source compositions and geodynamic implications. *Contributions to Mineralogy and Petrology* **140**, 263–282.

Shinjoe, H. (1997). Origin of the granodiorite in the forearc region of southwest Japan: melting of the Shimanto accretionary prism. *Chemical Geology* **134**, 237–255.

Shinjoe, H. & Sumii, T. (2001). Catalog of the Middle Miocene igneous rocks in the forearc region of the Southwest Japan: (2) Shikoku district. *Memoir of Human and Natural Sciences, Tokyo Keizai University* **112**, 51–91.

Shiraki, K., Yoshioka, K. & Matsumoto, Y. (1995). Magnesian andesites in the Oono volcanic rocks, central Kyusyu: westward continuation of the Setouchi volcanic belt. *Journal of the Geological Society of Japan* **101**, 387–392.

Shirey, S. B. & Hanson, G. N. (1984). Mantle-derived Archaean monzodiorites and trachyandesites [modified]. *Nature* **310**, 222–224.

Steiger, R. H. & Jäger, E. (1977). Subcommission on geochronology; convention on the use of decay constants in geo- and cosmochronology. *Earth and Planetary Science Letters* **36**, 359–362.

Stern, R. A. & Hanson, G. N. (1991). Archean high-Mg granodiorite; a derivative of light rare earth element-enriched monzodiorite of mantle origin. *Journal of Petrology* **32**, 201–238.

Stern, R. A., Hanson, G. N. & Shirey, S. B. (1989). Petrogenesis of mantle-derived, LILE-enriched Archean monzodiorites and trachyandesites (sanukitoids) in southwestern Superior Province. *Canadian Journal of Earth Sciences* **26**, 1688–1712.

Sumii, T. (2000). K–Ar ages of the Miocene Setouchi volcanic rocks in the western Setouchi Island Sea region, Southwest Japan. *Journal of the Geological Society of Japan* **106**, 609–619.

Suzuki, K. & Tatsumi, Y. (2003). Re–Os systematics of high-Mg andesites and basalts in the Setouchi volcanic belt, SW Japan: implications for mantle–melt interaction. *Frontier Research on Earth Evolution* **1** (in press).

Takahashi, E. (1986). Genesis of calc-alkali andesite magma in a hydrous mantle–crust boundary; petrology of lherzolite xenoliths from the Ichinomegata Crater, Oga Peninsula, Northeast Japan; Part II. *Journal of Volcanology and Geothermal Research* **29**, 355–395.

Takaoka, N. (1989). Problem in K–Ar dating of Quaternary volcanic rocks. *Journal of the Mass Spectrometry Society of Japan* **37**, 343–351.

Tamaki, K., Hsieh, K. Y., Tamura, C., Yamaashi, T. & Sasaki, T. (1999). High resolution reconstruction of the spreading tectonics of the Shikoku Basin in the Philippine Sea. *EOS Transactions, American Geophysical Union, Fall Meeting* **80**, 1040.

Tamura, Y., Yuhara, M. & Ishii, T. (2000). Primary arc basalts from Daisen volcano, Japan: equilibrium crystal fractionation versus disequilibrium fractionation during supercooling. *Journal of Petrology* **41**, 431–448.

Tatsumi, Y. (1981). Melting experiments on a high-magnesian andesite. *Earth and Planetary Science Letters* **54**, 357–365.

Tatsumi, Y. (1982). Origin of high-magnesian andesites in the Setouchi volcanic belt, Southwest Japan; II, Melting phase relations at high pressures. *Earth and Planetary Science Letters* **60**, 305–317.

Tatsumi, Y. (1983). High magnesian andesites in the Setouchi volcanic belt, Southwest Japan and their possible relation to the evolutionary history of the Shikoku inter-arc basin. In: Hilde, T. W. C. & Uyeda, S. (eds) *Geodynamics of the Western Pacific–Indonesian Region. Geodynamics Series, American Geophysical Union* **11**, 331–341.

Tatsumi, Y. (2001). Geochemical modeling of partial melting of subducting sediments and subsequent melt–mantle interaction: generation of high-Mg andesites in the Setouchi volcanic belt, southwest Japan. *Geology* **29**, 323–326.

Tatsumi, Y. & Eggins, S. (1995). *Subduction Zone Magmatism*. Oxford: Blackwell.

Tatsumi, Y. & Ishizaka, K. (1981). Existence of andesitic primary magma: an example from Southwest Japan. *Earth and Planetary Science Letters*, **53**, 124–130.

Tatsumi, Y. & Ishizaka, K. (1982). Magnesian andesite and basalt from Shodo-Shima island, southwest Japan, and their bearing on the genesis of calc-alkaline andesites. *Lithos* **15**, 161–172.

Tatsumi, Y. & Maruyama, S. (1989). Boninites and high-Mg andesites; tectonics and petrogenesis. In: Crawford, A. J. (ed.) *Boninites*. London: Unwin Hyman, pp. 50–71.

Tatsumi, Y., Torii, M. & Ishizaka, K. (1980). On the age of the volcanic activity and the distribution of the Setouchi volcanic rocks. *Bulletin of the Volcanological Society of Japan* **25**, 171–179.

Tatsumi, Y., Ishikawa, N., Anno, K., Ishizaka, K. & Itaya, T. (2001). Tectonic setting of high-Mg andesite magmatism in the SW Japan Arc; K–Ar chronology of the Setouchi volcanic belt. *Geophysical Journal International* **144**, 625–631.

Tatsumi, Y., Tamura, Y. & Nakashima, T. (2002). The petrology and geochemistry of calc-alkaline andesites on Shodo-Shima Island, SW Japan. *Journal of Petrology* **43**, 3–16.

Taylor, S. R. & McLennan, S. M. (1995). The geochemical evolution of the continental crust. *Reviews of Geophysics* **33**, 241–265.

Uto, K., Anno, K., Sudo, M. & Uchimizu, S. (1996). K–Ar ages for the Middle Miocene Muro volcanic rock, Southwest Japan. *Bulletin of the Volcanological Society of Japan* **41**, 257–261.

Yogodzinski, G. M., Volynets, O. N., Koloskov, A. V., Seliverstov, N. I. & Matvenkov, V. V. (1994). Magnesian andesites and the subduction component in a strongly calc-alkaline series at Piip Volcano, far western Aleutians. *Journal of Petrology* **35**, 163–204.

Yoshikawa, M., Shibata, T. & Tatsumi, Y. (2001). The Sr, Nd and Pb isotopic ratios of GSJ standard rocks. *Annual Report of Beppu Geothermal Research Laboratory, Kyoto University* **FY2000**, 30.